

Inhibition of double excitation and strong quantum entanglement via engineered cavity interactionsC. J. Zhu^{1,2,3}, W. Li², Y. P. Yang^{2,*} and G. S. Agarwal^{4,†}¹*School of Physical Science and Technology, Soochow University, Suzhou 215006, China*²*MOE Key Laboratory of Advanced Micro-Structured Materials, School of Physics Science and Engineering, Tongji University, Shanghai 200092, China*³*Collaborative Innovation Center of Light Manipulations and Applications, Shandong Normal University, Jinan 250358, China*⁴*Institute for Quantum Science and Engineering, Department of Biological and Agricultural Engineering, Department of Physics and Astronomy, Texas A&M University, College Station, Texas 77843, USA*

(Received 23 February 2022; revised 3 May 2022; accepted 1 December 2022; published 20 December 2022)

We propose a method for realizing the inhibition of simultaneous excitation of two identical qubits in a single-mode cavity QED system, where two qubits are driven by a coherent field and coupled to a cavity with engineered qubit-cavity interactions. By suitably chosen placements of the qubits in the cavity and by adjusting the relative decay strengths of the qubits and cavity field, we close many unwanted excitation pathways. This leads to an inhibition of the doubly excited state. In addition, we show that these two qubits are strongly entangled over a broad regime of the system parameters. We show that a strong signature of nonexcitation of the doubly excited state is the bunching property of the cavity photons, which thus provides a possible measurement of this nonexcitation. We also present dynamical features of the inhibition of simultaneous excitation of two qubits. The proposal presented in this paper can be realized not only in traditional cavity QED, but also in noncavity topological photonics involving edge modes.

DOI: [10.1103/PhysRevA.106.063713](https://doi.org/10.1103/PhysRevA.106.063713)**I. INTRODUCTION**

The inhibition of simultaneous excitation of two qubits was first investigated in free space [1], where two atoms far apart from each other are immersed in a laser field. If two atoms have different resonant frequencies, the doubly excited state cannot be excited due to the destructive interference between two excitation pathways in two-photon absorption. Several schemes have been suggested to allow the disallowed transitions [1–6].

Another method to prevent the excitation of two qubits is based on the van der Waals (vdW) interaction between two atoms in Rydberg states. Due to the vdW interaction, the doubly excited state will be shifted, preventing the absorption of two photons [7,8]. Thus only a single atom can be excited, and simultaneous excitation of two atoms is blocked. This effect is widely known as the dipole blockade or Rydberg blockade [9–11], which is the more pronounced the stronger the vdW interaction is. Moreover, the dipole blockade will result in many extraordinary phenomena, such as entangled atoms [12–15], super-radiance behavior [16], blockade gate operation [17–19], enhanced Kerr nonlinearity [20,21], and so on.

A similar phenomenon to generate the single-excitation state can also be realized in a two-identical-qubit system with strong dipole-dipole interaction [22]. In contrast to the Rydberg blockade, the effects of the dipole-dipole interaction

lead to the shift of the states from the single-qubit energy [5]. Thus the probability of simultaneously exciting two qubits can be suppressed when the double-excitation state is shifted from resonance by a single-photon resonant laser field. Since the suppression of two-photon excitation will not destroy the single-photon excitation, a single-excitation entangled state can be created, leading to a very large concurrence of two qubits [23,24].

In this paper, we propose a method to realize an inhibition of double excitation by engineering the qubit-cavity interactions instead of direct coupling between two qubits, and our proposal also yields a strong entanglement between two qubits. We consider a two-qubit cavity QED system with a π phase shift in positions of localized qubits as in the experiments of Refs. [16,25]. Under the strong-coupling regime, the symmetric Dicke state is decoupled from the cavity. When the cavity decay rate is much larger than the emitting rates of qubits, the excitation of the doubly excited state can be inhibited just by adjusting the quality factor of the cavity. Moreover, it is possible to observe this cavity-induced inhibition of exciting two qubits simultaneously by measuring the second-order photon correlation function. In the presence of this phenomenon, we also show that very strong entanglement between two qubits can be achieved. We add that an earlier work [26] considered steady-state production of entangled states of two atoms using cavity decay in a pair of lambda systems. The entangled states involved two lower states of the lambda system which are stable states. In contrast, we engineer cavity QED parameters to produce steady-state entanglement which involves two-level systems with a decaying excited state.

*Corresponding author: yang_yaping@tongji.edu.cn

†Corresponding author: girish.agarwal@tamu.edu

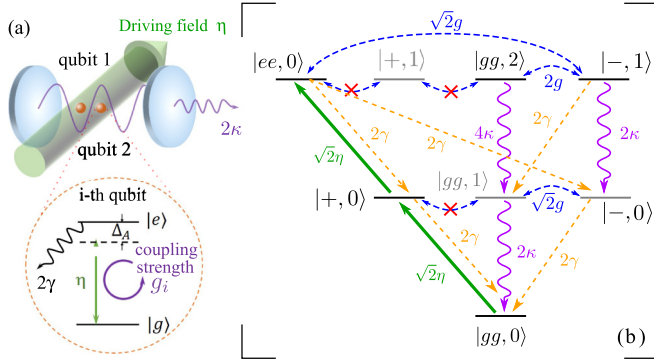


FIG. 1. (a) Schematic diagram of a single-mode cavity coupled with two qubits driven by a pump field with angular frequency ω_p and driving strength η . The decay rate of each qubit is 2γ , and the cavity decay rate is 2κ . The coupling strength of the i th qubit is g_i ($i = 1-2$), satisfying $g_1 = -g_2 = g_0$. (b) Physical picture leading to the suppression of double excitation. Here, we just show the main transition pathways and qubit-cavity interactions for this two-qubit QED system. The physical picture requires that the population of the state $|ee, 0\rangle$ should be quickly transferred to the cavity mode as we need to keep γ very low so that the state $|+, 0\rangle$ is significantly populated.

II. THEORETICAL MODEL

As shown in Fig. 1(a), we consider a scheme consisting of two identical qubits with resonant frequency ω_A in a single-mode cavity, where the cavity resonant frequency is ω_C , and two qubits are localized at different positions with a π phase shift, yielding $g_1 = -g_2 = g_0$. A pump field drives these two qubits directly with angular frequency ω_p and driving strength η . Under the rotating-wave approximation, the Hamiltonian of the system can be expressed as $H = H_0 + H_I + H_L$ with $H_0 = \hbar\Delta_A(S_z^{(1)} + S_z^{(2)})/2 + \hbar\Delta_C a^\dagger a$, $H_I = \hbar g_0[(a^\dagger S_-^{(1)} + a S_+^{(1)}) - (a^\dagger S_-^{(2)} + a S_+^{(2)})]$, and $H_L = \hbar\eta \sum_{i=1,2} (S_-^{(i)} + S_+^{(i)})$. Here, $\Delta_A = \omega_A - \omega_p$ and $\Delta_C = \omega_C - \omega_p$ are the detunings for the cavity and qubits, respectively. The operator a^\dagger (a) is the photon creation (annihilation) operator, while operators $S_z^{(i)}$ and $S_\pm^{(i)}$ are the spin operators of the i th ($i = 1, 2$) qubit.

In Fig. 1(b), we show the physical mechanism behind the inhibition of the doubly excited state. Figure 1(b) is based on the use of collective states for two qubits. We illustrate the possible transitions, and the diagram also shows the condition needed to realize the inhibition of double excitation. Using the collective states $|gg\rangle$, $|\pm\rangle = (|eg\rangle \pm |ge\rangle)/\sqrt{2}$ and $|ee\rangle$ as the basis, the Hamiltonian can be expressed in terms of the collective operators $D_z = S_z^{(1)} + S_z^{(2)}$ and $D_\pm^\dagger = (S_+^{(1)} \pm S_+^{(2)})/\sqrt{2}$, yielding $H_0 = \hbar\Delta_A D_z/2 + \hbar\Delta_C a^\dagger a$, $H_L = \sqrt{2}\hbar\eta(D_+^\dagger + D_+)$, and $H_I = 2\hbar g_0(aD_-^\dagger + a^\dagger D_-)/\sqrt{2}$. Here, the symmetric and antisymmetric Dicke states $|\pm\rangle$ are created by using the collective Dicke operators D_\pm^\dagger [8,27]. Assuming $\Delta_A = \Delta_C = 0$, one can obtain a clear picture of transition pathways for this two-qubit cavity QED system. As shown in Fig. 1(b), the symmetric Dicke state $|+, 0\rangle$ can be excited by absorbing a single photon (i.e., $|gg, 0\rangle \xrightarrow{\sqrt{2}\eta} |+, 0\rangle$). Due to the antisymmetric coupling (i.e., $g_1 = -g_2$), the symmetric Dicke state $|+, 0\rangle$

is decoupled from other states in the one-photon space. By absorbing another photon, the state $|ee, 0\rangle$ can be excited. In the two-photon space, possible qubit-cavity interactions are then via the coupling $|ee, 0\rangle \xleftrightarrow{\sqrt{2}g_0} |-, 1\rangle \xleftrightarrow{2g_0} |gg, 2\rangle$. When the cavity decay rate is much larger than the emitting rates of qubits (i.e., $\kappa \gg \gamma$), the population of the doubly excited state should be quickly transferred to the cavity mode. Therefore the probability of detecting the symmetric Dicke state $|+, 0\rangle$ is predominant, yielding nonexcitation of the state $|ee, 0\rangle$ via the engineered environment and qubit-cavity interactions. It is worth pointing out that this inhibition of the simultaneous excitation of two identical qubits can also be detected by measuring the second-order photon correlation function $g^{(2)}(0) = \langle a^\dagger a^\dagger a a \rangle / (\langle a^\dagger a \rangle)^2$. Since the photons leak from the cavity via the state $|gg, 2\rangle$, strong bunching of photons [i.e., $g^{(2)}(0) > 2$] can be observed with nonexcitation of state $|ee, 0\rangle$.

III. BIEXCITATION BLOCKADE-QUANTITATIVE TREATMENT

We next present full master equation calculations to confirm the physical picture as outlined in Fig. 1(b). To show this inhibition of the excitation of two qubits quantitatively, one can directly solve the master equation

$$\frac{d}{dt}\rho = -i[H_0 + H_I + H_L, \rho] + \mathcal{L}_\kappa\rho + \mathcal{L}_\gamma\rho, \quad (1)$$

where ρ is the density matrix operator of the system. The damping terms of the cavity and qubits are given by $\mathcal{L}_\kappa\rho = \kappa(2a\rho a^\dagger - a^\dagger a\rho - \rho a^\dagger a)$ and $\mathcal{L}_\gamma\rho = \gamma \sum_{i=1,2} (2S_-^{(i)}\rho S_+^{(i)} - S_+^{(i)}S_-^{(i)}\rho - \rho S_+^{(i)}S_-^{(i)})$, respectively. The inhibition of double excitation can be characterized by evaluating the ratio between the double-excitation probability and the square of the single-excitation probability, i.e.,

$$\xi \equiv P_{ee}/P_e^2, \quad (2)$$

under the steady-state condition. Here, $P_{ee} = \langle ee|\rho_{\text{atom}}|ee\rangle$ is the probability of finding two qubits excited, and $P_e = \langle e|\rho_{\text{atom1}}|e\rangle = \langle e|\rho_{\text{atom2}}|e\rangle$ denotes the probability of finding one of two qubits excited. In the presence of the inhibition of double excitation, the probability of detecting the doubly excited state is smaller than that of detecting the single-qubit excitation state. Therefore the value of ξ is smaller than unity, giving a direct signature of the suppression of the double excitation. The stronger the suppression of double excitation becomes, the smaller the ratio ξ is.

First, we study the probability of detecting the doubly excited state P_{ee} as a function of the normalized coupling strength g_0/κ in Fig. 2(a). The qubit decay rate is chosen as $\gamma/\kappa = 1$ (dotted blue curve), 0.1 (dashed green curve), 0.01 (dash-dotted orange curve), and 0.001 (solid purple curve). Other system parameters are given by $\eta/\gamma = 5$ and $\Delta_A = \Delta_C = 0$. In our numerical simulation, the number of photon states is chosen to be 50 to ensure the convergence of the numerical procedure. In the case of $\kappa \gg \gamma$, the value of P_{ee} [dash-dotted orange and solid purple curves shown in Fig. 2(a)] drops significantly as the qubit-cavity coupling strength increases. This is because the strong qubit-cavity interaction $|ee, 0\rangle \xleftrightarrow{\sqrt{2}g_0} |-, 1\rangle \xleftrightarrow{2g_0} |gg, 2\rangle$ opens an additional

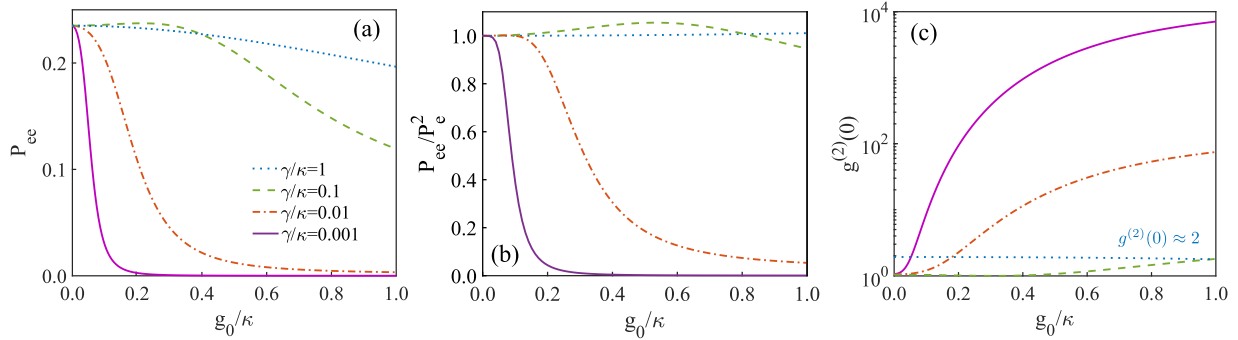


FIG. 2. The probability of detecting the doubly excited state P_{ee} (a), the ratio ξ (b), and the second-order photon correlation function $g^{(2)}(0)$ (c) as a possible method for detection in experiments. Here, the qubit decay rate is chosen as $\gamma/\kappa = 1$ (dotted blue curve), 0.1 (dashed green curve), 0.01 (dash-dotted orange curve), and 0.001 (solid purple curve). Other system parameters are given by $\Delta_A = \Delta_C = 0$ and $\eta = 5\gamma$.

damping pathway and the decay of state $|gg, 2\rangle$ becomes predominant. However, the symmetric Dicke state $|+, 0\rangle$ uncouples from other states in the one-photon space due to the antisymmetric coupling. Thus it is stable, and the inhibition of double excitation occurs, yielding $\xi < 1$ as shown in Fig. 2(b). In the case of $\kappa \leq \gamma$, the doubly excited state $|ee, 0\rangle$ is as stable as the single-excitation state $|+, 0\rangle$. Thus the suppression of double excitation disappears, and the ratio $\xi \approx 1$ [see dotted blue and dashed green curves in Fig. 2(b)]. In the presence of nonexcitation of the doubly excited state, the second-order photon correlation function $g^{(2)}(0) > 2$ shown in Fig. 2(c), and extremely strong bunching of photons can be detected.

In Fig. 3(a), we also show the value of $\log_{10}(\xi)$ as functions of the normalized qubit-cavity coupling strength g_0/κ and the detuning Δ_C/κ , respectively. Here, we choose $\omega_C = \omega_A$, $\gamma/\kappa = 0.01$, and $\eta = 5\gamma$. It is noted that the engineered-interaction-and-environment-induced nonexcitation of the doubly excited state only occurs in the resonant or near-resonant driving regime. As the qubit-cavity coupling strength g_0 increases, the frequency regime for realizing the inhibition of doubly excitation is broadened simultaneously, which provides great facilities for experimental implementation.

IV. REMOTE ENTANGLEMENT OF TWO QUBITS

As demonstrated in Ref. [11], the strong entanglement of two qubits can be achieved when the double excitation is

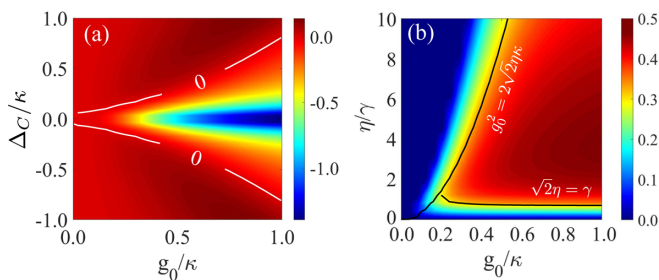


FIG. 3. (a) The value of $\log_{10}(\xi)$ as functions of the normalized coupling strength g_0/κ and detuning Δ_C/κ with $\omega_C = \omega_A$. The white curves indicate $\log_{10}(\xi) = 0$. (b) The concurrence as functions of the normalized coupling strength g_0/κ and driving intensity η/γ , respectively. Here, the black curves denote the boundary of the two strongly entangled qubits, where the concurrence is close to 0.5.

inhibited. To show this interesting property, we evaluate the concurrence of two qubits under the steady-state condition, where the maximum value of the concurrence is 0.5. As shown in Fig. 3(b), there exists a regime where these two qubits are strongly entangled (red region). The boundaries denoted by the black curves are given by $g_0^2 = 2\sqrt{2}\eta\kappa$ and $\sqrt{2}\eta = \gamma$, respectively (see Appendix A for details). Here, the system parameters are chosen as $\Delta_A = \Delta_C = 0$, $\gamma = 0.01\kappa$. It is clear to see that the value of the concurrence tends to be saturated when the coupling strength g_0 is large enough. Then, we choose $g_0 = \kappa$ and scan the driving field intensity to show the influence of qubit decay rate on the entanglement of two qubits. In Fig. 4, the maximum value of the concurrence is calculated as a function of the normalized qubit decay rate γ/κ . Clearly, strong entanglement can be achieved when the qubit decay rate is much smaller than the cavity decay rate, e.g., the ratio $\gamma/\kappa \ll 0.01$. Except for the concurrence, the entanglement of two qubits can also be demonstrated by evaluating the real parts of the elements of the qubit density matrix ρ_{qubit} . When the ratio $\gamma/\kappa \gtrsim 1$, the system is in the ground state $|gg\rangle$ in the equilibrium condition. However, in the case of $\gamma/\kappa \ll 1$, the system is in a mixture state consisting of a ground state with weight 0.5 and a single-qubit excitation state $(|eg\rangle + |ge\rangle)/\sqrt{2}$ as depicted by the orange bars with qubit decay rate $\gamma = 10^{-3}\kappa$.

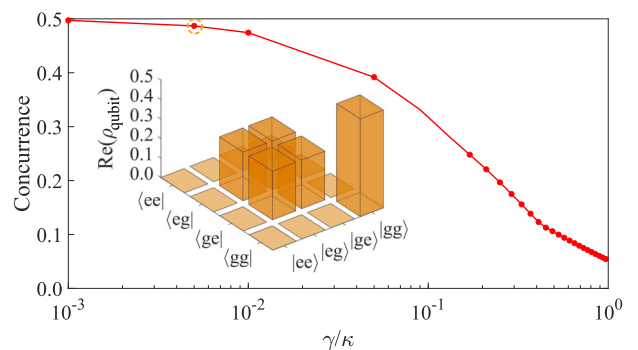


FIG. 4. The red curve represents the steady-state concurrence against the qubit decay rate γ/κ with $g_0 = \kappa$. The orange bar diagram demonstrates the real part of the qubit density matrix elements with $\gamma = 5 \times 10^{-3}\kappa$ (dashed orange circle).

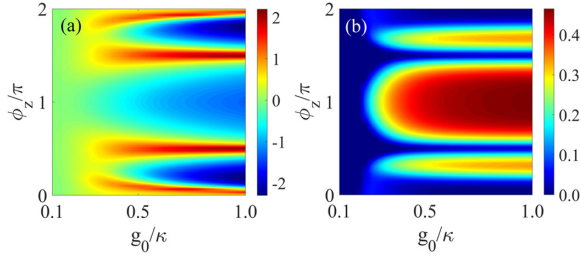


FIG. 5. The variable $\log_{10}(\xi)$ (a) and the steady-state concurrence (b) are plotted as functions of the normalized coupling strength g_0/κ and the position-dependent phase difference ϕ_z/π between two qubits. Here, we set $\gamma = 0.01\kappa$, $\Delta_A = \Delta_C = 0$, and $\eta = 5\gamma$ for the numerical calculation.

Next, let us investigate how exclusive the condition of $g_1 = -g_2$ is to realize this engineered-interaction-and-environment-induced inhibition of double excitation and the corresponding entanglement of the two qubits. We first assume that one qubit is trapped at the peak of the cavity mode with a qubit-cavity coupling strength $g_1 = g_0$ for mathematical simplicity. Then, the coupling strength of the other qubit is given by $g_2 = g_0 \cos(\phi_z)$, where $\phi_z = 2\pi\Delta_z/\lambda_C$ is the position-dependent phase shift with Δ_z being the distance between two qubits and λ_C being the wavelength of the cavity mode. In Fig. 5, we plot the ratio $\log_{10}(\xi)$ [Fig. 5(a)] and the concurrence [Fig. 5(b)] as functions of the normalized coupling strength g_0/κ and the phase difference ϕ_z/π , respectively. Here, we choose $\gamma = 0.01\kappa$, and other system parameters are the same as those used in Fig. 4. It is noted that the engineered-interaction-and-environment-induced inhibition of double excitation (i.e., $\xi < 1$) and strong entanglement between two qubits (the concurrence is close to 0.5) can be achieved over a wide regime of coupling strengths near the π phase shift, which is robust for experimental implementation. However, note that if one is interested in the smallest possible double excitation, then phase $\pi/4$ is preferable. We also notice that the engineered-interaction-and-environment-induced inhibition of double excitation *cannot* be realized in the case of $g_1 = g_2$ since the interaction between states $|+, 0\rangle$ and $|gg, 1\rangle$ is allowed. More details are given in Appendix B.

Finally, we discuss the dynamical properties of this engineered-interaction-and-environment-induced inhibition of double excitation and the corresponding entanglement of two qubits by numerically solving the time-dependent master equation with the initial condition $P_{gg} = 1$. In Fig. 6(a), we show the probability of detecting the doubly excited state P_{ee} as a function of the normalized time parameter γt with different qubit decay rate $\gamma = \kappa$ (dash-dotted green curve), 0.1κ (dashed orange curve), 0.01κ (dotted blue curve), and 0.001κ (solid red curve). Other system parameters are chosen as $g_0 = \kappa$, $\eta = 5\gamma$, and $\Delta_A = \Delta_C = 0$. Obviously, the probability of finding a doubly excited state reaches over 50% in the case of $\gamma = \kappa$. As the qubit decay rate decreases, however, the probability of finding a doubly excited state drops quickly. In particular, the double excitation will be significantly inhibited when $\gamma \ll \kappa$ [see dotted blue and solid red curves in the inset of Fig. 6(a)]. The oscillation in P_{ee} can be explained by describing the system

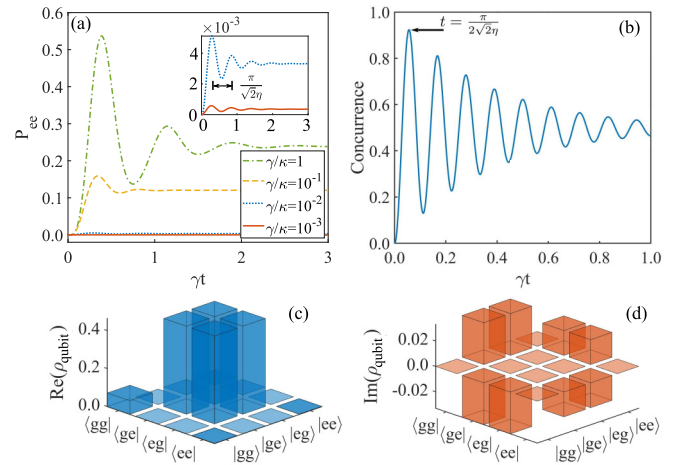


FIG. 6. (a) The probability of detecting doubly excited state P_{ee} vs the normalized evolution time γt with the initial condition $P_{gg} = 1$. The qubit decay rate is chosen as $\gamma = \kappa$ (dash-dotted green curve), $10^{-1}\kappa$ (dashed orange curve), $10^{-2}\kappa$ (dotted blue curve), and $10^{-3}\kappa$ (solid red curve), respectively. Other system parameters are given by $\Delta_A = \Delta_C = 0$, $g_0 = \kappa$, and $\eta = 5\gamma$. The inset in (a) only shows the results of $\gamma/\kappa = 10^{-2}$ (dotted blue curve) and 10^{-3} (solid red curve). (b) The concurrence is plotted as a function of time with $\gamma/\kappa = 10^{-3}$ and $\eta = 20\gamma$. (c) and (d) The blue (c) and red (d) bars demonstrate the real and imaginary parts of the qubit density matrix at $t = \pi/(2\sqrt{2}\eta)$, respectively.

as a damping two-level model. Using the time-dependent Bloch equations, the probability of detecting the doubly excited state oscillates with a period of time $\pi/(\sqrt{2}\eta)$ (see Appendix C). Likewise, the concurrence has similar dynamical characteristics exhibited in the profile of P_{ee} . As shown in Fig. 6(b), the concurrence also oscillates with a period of time $\pi/(\sqrt{2}\eta)$ and reaches its maximum at time $t = \pi/(2\sqrt{2}\eta)$, corresponding to a maximum entanglement of two qubits. Here, we choose the system parameters as $\gamma = 10^{-3}\kappa$, $g_0 = 4\kappa$, and $\eta = 20\gamma$. The maximum value of the concurrence is close to 0.93 at $t \approx 0.06/\gamma$. The corresponding real (blue bars) and imaginary parts (red bars) of the elements of the atomic density matrix ρ_{qubit} are demonstrated in Figs. 6(c) and 6(d), respectively. Clearly, the probabilities of finding single-qubit excited states are predominant compared with probabilities of finding qubits in other states. More importantly, these states are stable since their imaginary parts are zero.

Before ending, let us discuss the feasibility of the experimental implementation of this two-qubit cavity QED system with engineered qubit-cavity interactions and environment. With current experimental technologies, a spatial π phase difference of two qubits can be achieved not only in traditional cavity QED systems [16,25] but also in noncavity topological photonics involving edge modes [28,29]. A possible platform to realize our proposal is the semiconductor quantum dot QED system, where ideal decay rates of quantum dots in such systems are of the order of 0.1 GHz, but the interaction strengths and cavity field decay rates are about two orders of magnitude bigger [30].

V. CONCLUSION

In conclusion, we provide a physical mechanism for inhibition of double excitation by using engineered interactions and an engineered environment. To realize this phenomenon, the positions of two qubits are chosen suitably, and the decay strengths of the cavity field and qubits satisfy $\kappa \gg \gamma$. For example, in the case of a spatial π phase shift in the positions of the localized qubits, the symmetric Dicke state is decoupled from other states in the one-photon space, and the population of the doubly excited state is transferred quickly to the cavity mode. Thus the symmetric Dicke state is significantly populated, resulting in the elimination of double excitation. Moreover, this effect can be detected by measuring the second-order photon correlation function. In the presence of the inhibition of double excitation, extremely strong bunching of photons can be observed. Using the mean-field method, we also show that the strong entanglement of two qubits can be achieved under the conditions of $g_0^2 \geq 2\sqrt{2}\eta\kappa$ and $\sqrt{2}\eta \gg \gamma$.

ACKNOWLEDGMENTS

C.J.Z. thanks Prof. H. Chen at Tongji University for fruitful discussions. C.J.Z. and Y.P.Y. thank the National Natural Science Foundation of China (Grants No. 61975154 and No. 12274326) and the National Key Research and Development Program of China (Grants No. 2021YFA1400600 and No. 2021YFA1400602) for support. G.S.A. thanks the Air Force Office of Scientific Research (Award No. FA9550-20-1-0366) for support.

APPENDIX A: MEAN-FIELD APPROXIMATION

As shown in Fig. 1(b), the state $|gg, 2\rangle$ is coupled with the doubly excited state $|ee, 0\rangle$ via the qubit-cavity interaction. Thus the mean photon number is nonzero. To show this point, we explore the nonzero solution for mean photon number by solving the Heisenberg equations of motion for operators. Under the mean-field approximation, we have

$$\langle \dot{a} \rangle = -i\Delta_C \langle a \rangle - ig_0(\langle S_-^{(1)} \rangle - \langle S_-^{(2)} \rangle) - \kappa \langle a \rangle, \quad (\text{A1a})$$

$$\langle S_-^{(1)} \rangle = -i\frac{\Delta_A}{2} \langle S_-^{(1)} \rangle + 2ig_0 \langle a \rangle \langle S_z^{(1)} \rangle + 2i\eta \langle S_z^{(1)} \rangle - \gamma \langle S_-^{(1)} \rangle, \quad (\text{A1b})$$

$$\langle S_-^{(2)} \rangle = -i\frac{\Delta_A}{2} \langle S_-^{(2)} \rangle - 2ig_0 \langle a \rangle \langle S_z^{(2)} \rangle + 2i\eta \langle S_z^{(2)} \rangle - \gamma \langle S_-^{(2)} \rangle, \quad (\text{A1c})$$

$$\langle S_z^{(1)} \rangle = ig_0(\langle a^\dagger \rangle \langle S_-^{(1)} \rangle - \langle a \rangle \langle S_+^{(1)} \rangle) - i\eta(\langle S_+^{(1)} \rangle - \langle S_-^{(1)} \rangle) - \gamma(1 + 2\langle S_z^{(1)} \rangle), \quad (\text{A1d})$$

$$\langle S_z^{(2)} \rangle = ig_0(\langle a \rangle \langle S_+^{(2)} \rangle - \langle a^\dagger \rangle \langle S_-^{(2)} \rangle) - i\eta(\langle S_+^{(2)} \rangle - \langle S_-^{(2)} \rangle) = -\gamma(1 + 2\langle S_z^{(2)} \rangle), \quad (\text{A1e})$$

where $\langle \mathcal{O} \rangle$ corresponds to the expectation value of the operator \mathcal{O} . Assuming $\Delta_A = \Delta_C = 0$, Eqs. (A1a)–(A1e) have a trivial photon number solution with $a = 0$, and $S_-^{(j)} =$

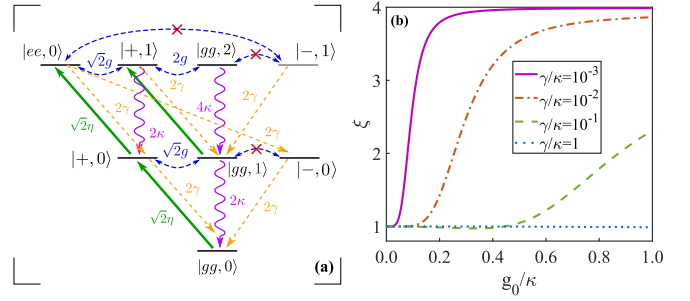


FIG. 7. (a) Transition pathways for the case of $g_1 = g_2$. (b) The ratio ξ vs the normalized coupling strength g_0/κ with $\gamma/\kappa = 10^{-3}$ (solid purple curve), 10^{-2} (dash-dotted orange curve), 10^{-1} (dashed green curve), and 1 (dotted blue curve), respectively.

$2i\eta S_z^{(j)}/\gamma$ and $S_z^{(j)} = -\gamma^2/[2(\gamma^2 + 2\eta^2)]$ ($j = 1-2$), respectively.

To obtain the nontrivial photon number solution, i.e., $\langle a \rangle \neq 0$, we set $\langle a \rangle = \alpha_{\text{Re}} + i\alpha_{\text{Im}}$ and insert it into Eqs. (A1a)–(A1e). Then, one can obtain $\alpha_{\text{Im}} = 0$ and

$$\langle S_z^{(1)} \rangle = -\gamma \left/ \left(2\gamma + \frac{4g_0^2 \alpha_{\text{Re}}^2}{\gamma} + \frac{4\eta^2}{\gamma} + \frac{8g_0\eta\alpha_{\text{Re}}}{\gamma} \right) \right., \quad (\text{A2a})$$

$$\langle S_z^{(2)} \rangle = -\gamma \left/ \left(2\gamma + \frac{4g_0^2 \alpha_{\text{Re}}^2}{\gamma} + \frac{4\eta^2}{\gamma} - \frac{8g_0\eta\alpha_{\text{Re}}}{\gamma} \right) \right., \quad (\text{A2b})$$

$$\begin{aligned} & \frac{2g_0\eta}{\gamma} (\langle S_z^{(2)} \rangle - \langle S_z^{(1)} \rangle) \\ &= \alpha_{\text{Re}} \left[\frac{2g_0^2}{\gamma} (\langle S_z^{(1)} \rangle + \langle S_z^{(2)} \rangle) - \kappa \right]. \end{aligned} \quad (\text{A2c})$$

Inserting Eqs. (A2a) and (A2b) into Eq. (A2c), we can obtain

$$\alpha_{\text{Re}} = \pm \sqrt{\frac{2\eta^2\kappa - (g_0^2 + \kappa\gamma)\gamma + \gamma\sqrt{g_0^4 - 8\eta^2\kappa^2}}{2g_0^2\kappa}}. \quad (\text{A3})$$

Note that Eq. (A3) is only valid for $g_0^2 \geq 2\sqrt{2}\eta\kappa$ and $\sqrt{2}\eta \geq \gamma$, which are the boundaries of the strong concurrence shown in Fig. 3.

APPENDIX B: THE CASE OF $g_1 = g_2$

For the case of $g_1 = g_2 = g_0$, the interaction Hamiltonian can be expressed as $H_I = 2\hbar g_0(aD_+^\dagger + a^\dagger D_+)/\sqrt{2}$. Thus the single-qubit excitation state $|+, 0\rangle$ is then coupled with the single-photon state $|gg, 1\rangle$ as shown in Fig. 7. Since the transition pathway $|+, 0\rangle \leftrightarrow |gg, 1\rangle$ is allowed, the state $|+, 1\rangle$ becomes unstable, and the driving field results in $|gg, 1\rangle \xrightarrow{\sqrt{2}\eta} |+, 1\rangle$ transition, leading to double excitation via the $|+, 1\rangle \leftrightarrow |ee, 0\rangle$ transition pathway. Therefore the parameter $\xi \geq 1$ as shown in Fig. 7(b).

APPENDIX C: REDUCED TWO-LEVEL MODEL

Since the doubly excited state is inhibited, the system can be reduced to a two-level system with energy levels $|1\rangle \equiv$

$|gg, 0\rangle$ and $|2\rangle \equiv |+, 0\rangle$. These two states are coupled via a coherent field with effective Rabi frequency $\sqrt{2}\eta$. Thus the Bloch equations describing the dynamics of this resonantly driven two-level model are given by

$$i\frac{\partial}{\partial t}\rho_{11} - 2i\gamma\rho_{22} + \sqrt{2}\eta(\rho_{21} - \rho_{12}) = 0, \quad (\text{C1a})$$

$$i\frac{\partial}{\partial t}\rho_{22} + 2i\gamma\rho_{22} - \sqrt{2}\eta(\rho_{21} - \rho_{12}) = 0, \quad (\text{C1b})$$

$$i\frac{\partial}{\partial t}\rho_{12} + i\gamma\rho_{12} + \sqrt{2}\eta(\rho_{22} - \rho_{11}) = 0. \quad (\text{C1c})$$

Solving Eqs. (C1a)–(C1c) with the initial condition $\rho_{11}(0) = 1$ and $\rho_{22}(0) = 0$, one can easily obtain the time-dependent populations in states $|gg, 0\rangle$ and $|+, 0\rangle$, which read

$$\rho_{11}(t) = \frac{2\eta^2(K_-e^{K_+t} - K_+e^{K_-t}) + (K_+ - K_-)(2\eta^2 + \gamma^2)}{(K_- - K_+)(4\eta^2 + \gamma^2)}, \quad (\text{C2a})$$

$$\rho_{22}(t) = \frac{2\eta^2[(K_- - K_+) + (K_-e^{K_+t} - K_+e^{K_-t})]}{(K_- - K_+)(4\eta^2 + \gamma^2)}, \quad (\text{C2b})$$

with $K_{\pm} \equiv -(3\gamma \pm \sqrt{\gamma^2 - 32\eta^2})/2$. Under the condition of $\eta \gg \gamma$, one can easily obtain $\rho_{11}(t) \approx [1 + \cos(2\sqrt{2}\eta t)]/2$ and $\rho_{22}(t) \approx [1 - \cos(2\sqrt{2}\eta t)]/2$. Thus the density matrix elements ρ_{11} and ρ_{22} oscillate with a period of $\pi/(\sqrt{2}\eta)$. To verify the above analysis, we compare the numerical result by

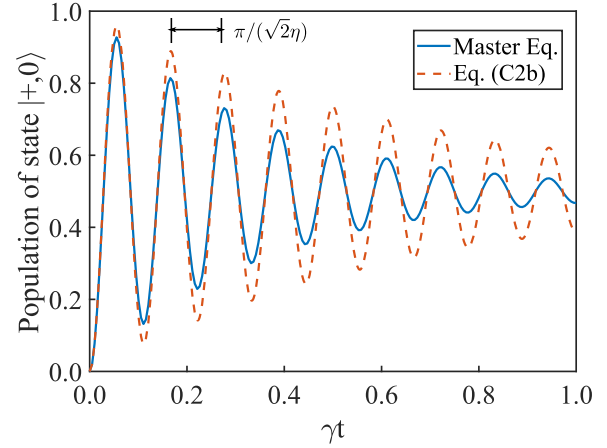


FIG. 8. Comparison between the numerical result (solid blue curve) obtained by solving the master equation and the analytical result (dashed orange curve) from Eq. (C2b).

solving the master equation with the result from Eq. (C2b). As shown in Fig. 8, these two results match well except for their amplitudes. This is because the states in two-photon space attribute more decay pathways and quantum fluctuations are not included in this reduced two-level model. Thus the amplitude of the numerical result (solid blue curve) is a little smaller than that of the analytical result (dashed orange curve).

- [1] A. Muthukrishnan, G. S. Agarwal, and M. O. Scully, Inducing Disallowed Two-Atom Transitions with Temporally Entangled Photons, *Phys. Rev. Lett.* **93**, 093002 (2004).
- [2] G. V. Varada and G. S. Agarwal, Two-photon resonance induced by the dipole-dipole interaction, *Phys. Rev. A* **45**, 6721 (1992).
- [3] Z. Zheng, P. L. Saldanha, J. R. Rios Leite, and C. Fabre, Two-photon–two-atom excitation by correlated light states, *Phys. Rev. A* **88**, 033822 (2013).
- [4] W. Ren, W. Liu, C. Song, H. Li, Q. Guo, Z. Wang, D. Zheng, G. S. Agarwal, M. O. Scully, S.-Y. Zhu, H. Wang, and D.-W. Wang, Simultaneous Excitation of Two Noninteracting Atoms with Time-Frequency Correlated Photon Pairs in a Superconducting Circuit, *Phys. Rev. Lett.* **125**, 133601 (2020).
- [5] C. Hettich, C. Schmitt, J. Zitzmann, S. Kuhn, I. Gerhardt, and V. Sandoghdar, Nanometer resolution and coherent optical dipole coupling of two individual molecules, *Science* **298**, 385 (2002).
- [6] A. Vivas-Viaña and C. Sanchez Muñoz, Two-photon resonance fluorescence of two interacting nonidentical quantum emitters, *Phys. Rev. Res.* **3**, 033136 (2021).
- [7] M. O. Scully and M. S. Zubairy, *Quantum Optics* (Cambridge University Press, Cambridge, 1999).
- [8] G. Agarwal, *Quantum Optics* (Cambridge University Press, Cambridge, 2012).
- [9] E. Urban, T. A. Johnson, T. Henage, L. Isenhower, D. D. Yavuz, T. G. Walker, and M. Saffman, Observation of Rydberg blockade between two atoms, *Nat. Phys.* **5**, 110 (2009).
- [10] M. Saffman, T. G. Walker, and K. Mølmer, Quantum information with Rydberg atoms, *Rev. Mod. Phys.* **82**, 2313 (2010).
- [11] J. Gillet, G. S. Agarwal, and T. Bastin, Tunable entanglement, antibunching, and saturation effects in dipole blockade, *Phys. Rev. A* **81**, 013837 (2010).
- [12] T. Wilk, A. Gaëtan, C. Evellin, J. Wolters, Y. Miroshnychenko, P. Grangier, and A. Browaeys, Entanglement of Two Individual Neutral Atoms Using Rydberg Blockade, *Phys. Rev. Lett.* **104**, 010502 (2010).
- [13] H. Levine, A. Keesling, A. Omran, H. Bernien, S. Schwartz, A. S. Zibrov, M. Endres, M. Greiner, V. Vuletić, and M. D. Lukin, High-Fidelity Control and Entanglement of Rydberg-Atom Qubits, *Phys. Rev. Lett.* **121**, 123603 (2018).
- [14] T. M. Graham, M. Kwon, B. Grinkemeyer, Z. Marra, X. Jiang, M. T. Lichtman, Y. Sun, M. Ebert, and M. Saffman, Rydberg-Mediated Entanglement in a Two-Dimensional Neutral Atom Qubit Array, *Phys. Rev. Lett.* **123**, 230501 (2019).
- [15] I. S. Madjarov, J. P. Covey, A. L. Shaw, J. Choi, A. Kale, A. Cooper, H. Pichler, V. Schkolnik, J. R. Williams, and M. Endres, High-fidelity entanglement and detection of alkaline-earth Rydberg atoms, *Nat. Phys.* **16**, 857 (2020).
- [16] R. Reimann, W. Alt, T. Kampschulte, T. Macha, L. Ratschbacher, N. Thau, S. Yoon, and D. Meschede, Cavity-Modified Collective Rayleigh Scattering of Two Atoms, *Phys. Rev. Lett.* **114**, 023601 (2015).
- [17] M. Müller, I. Lesanovsky, H. Weimer, H. P. Büchler, and P. Zoller, Mesoscopic Rydberg Gate Based on Electromagnetically Induced Transparency, *Phys. Rev. Lett.* **102**, 170502 (2009).
- [18] K. M. Maller, M. T. Lichtman, T. Xia, Y. Sun, M. J. Piotrowicz, A. W. Carr, L. Isenhower, and M. Saffman, Rydberg-blockade

- controlled-NOT gate and entanglement in a two-dimensional array of neutral-atom qubits, *Phys. Rev. A* **92**, 022336 (2015).
- [19] D. Tiarks, S. Schmidt-Eberle, T. Stolz, G. Rempe, and S. Dürr, A photon–photon quantum gate based on Rydberg interactions, *Nat. Phys.* **15**, 124 (2019).
- [20] Z. Y. Bai and G. X. Huang, Enhanced third-order and fifth-order Kerr nonlinearities in a cold atomic system via Rydberg–Rydberg interaction, *Opt. Express* **24**, 4442 (2016).
- [21] J. Sinclair, D. Angulo, N. Lupu-Gladstein, K. Bonsma-Fisher, and A. M. Steinberg, Observation of a large, resonant, cross-Kerr nonlinearity in a cold Rydberg gas, *Phys. Rev. Res.* **1**, 033193 (2019).
- [22] K. Almutairi, R. Tanaś, and Z. Ficek, Generating two-photon entangled states in a driven two-atom system, *Phys. Rev. A* **84**, 013831 (2011).
- [23] M. D. Lukin and P. R. Hemmer, Quantum Entanglement via Optical Control of Atom-Atom Interactions, *Phys. Rev. Lett.* **84**, 2818 (2000).
- [24] Ö. Çakir, A. A. Klyachko, and A. S. Shumovsky, Steady-state entanglement of two atoms created by classical driving field, *Phys. Rev. A* **71**, 034303 (2005).
- [25] A. Neuzner, M. Körber, O. Morin, S. Ritter, and G. Rempe, Interference and dynamics of light from a distance-controlled atom pair in an optical cavity, *Nat. Photon.* **10**, 303 (2016).
- [26] M. J. Kastoryano, F. Reiter, and A. S. Sørensen, Dissipative Preparation of Entanglement in Optical Cavities, *Phys. Rev. Lett.* **106**, 090502 (2011).
- [27] M. O. Pleinert, J. Von Zanthier, and G. S. Agarwal, Hyper-radiance from collective behavior of coherently driven atoms, *Optica* **4**, 779 (2017).
- [28] J. Jiang, J. Ren, Z. W. Guo, W. W. Zhu, Y. Long, H. T. Jiang, and H. Chen, Seeing topological winding number and band inversion in photonic dimer chain of split-ring resonators, *Phys. Rev. B* **101**, 165427 (2020).
- [29] Z. Guo, T. Zhang, J. Song, H. Jiang, and H. Chen, Sensitivity of topological edge states in a non-Hermitian dimer chain, *Photon. Res.* **9**, 574 (2021).
- [30] D. Englund, A. Faraon, I. Fushman, N. Stoltz, P. Petroff, and J. Vuckovic, Controlling cavity reflectivity with a single quantum dot, *Nature (London)* **450**, 857 (2007).